

1 **The role of the timing of Sudden Stratospheric Warmings for precipitation**
2 **and temperature anomalies in Europe**

3

4 Erika Monnin¹, Marlene Kretschmer^{2,*}, Inna Polichtchouk³

5 ¹ENSTA Paris, Palaiseau, France

6 ²Department of Meteorology, University of Reading, Reading, UK

7 ³European Centre for Medium-Range Weather Forecasts, Shinfield Rd, Reading RG2 9AX, UK

8 *corresponding author, m.j.a.kretschmer@reading.ac.uk (@Marlene_Climate)

9

10 THIS VERSION WAS ACCEPTED FOR PUBLICATION AT THE *INTERNATIONAL JOURNAL OF CLIMATOLOGY*.

11

12 **Abstract**

13 The Northern Hemisphere stratospheric polar vortex (SPV), a band of fast westerly winds over the pole
14 extending from approximately 10 to 50 km altitude, is a key driver of European winter weather.
15 Extremely weak polar vortex states, so called sudden stratospheric warmings (SSWs), are on average
16 followed by dry and cold weather in Northern Europe, as well as wetter weather in Southern Europe.
17 However, the surface response of SSWs varies greatly between events, and it is not well understood
18 which factors modulate this difference. Here we address the role of the timing of SSWs within the cold
19 season (December to March) for the temperature and precipitation response in Europe. Given the
20 limited sample size of SSWs in the observations, hindcasts of the seasonal forecasting model SEAS5
21 from the European Centre for Medium-Range Weather Forecasts (ECMWF) are analysed. Firste
22 evaluate key characteristics of stratosphere-troposphere coupling in SEAS5 against reanalysis data and
23 find them to be reasonably well captured by the model, justifying our approach. We then show that in
24 SEAS5, early winter (December and January) SSWs are followed by more pronounced surface impacts
25 compared to late winter (February and March) SSWs. For example, in Scotland the low precipitation
26 anomalies are roughly twice as severe after early winter SSWs than after late winter SSWs. The
27 difference in the response cannot be explained by more downward propagating SSWs in early winter,
28 or by different monthly precipitation climatologies. Instead, we demonstrate that the differences
29 result from stronger SPV anomalies associated with early winter SSWs. This is a statistical artefact
30 introduced through the commonly used SSW event definition, which involves an absolute threshold,
31 and therefore leads to stronger SPV anomalies during early winter SSWs when the stratospheric mean
32 state is stronger. Our study highlights the sensitivity of surface impacts to SSW event definition.

33

34 **1 Introduction**

35 A key driver of European weather and climate is the Northern hemisphere stratospheric polar vortex
36 (SPV) (Baldwin and Dunkerton, 2001; Kretschmer *et al.*, 2018a, 2018b; King *et al.*, 2019; Domeisen and
37 Butler, 2020). The SPV is a band of strong westerly winds in the Arctic stratosphere which forms during
38 boreal autumn (Waugh *et al.*, 2016). It stems from a strong temperature gradient between the Arctic
39 and the lower latitudes due to the lack of incoming solar radiation over the Arctic during the cold
40 season, and it disappears again in spring when sunlight returns to the pole.

41 Extreme weak phases of the SPV, such as major sudden stratospheric warmings (SSWs), during which
42 the vortex breaks down and the winds in the stratosphere reverse, can affect the tropospheric
43 circulation below (Baldwin and Dunkerton, 2001; Waugh *et al.*, 2016). In particular, SSWs are often
44 followed by persistent negative phases of the North Atlantic Oscillation (NAO-) and the associated
45 weather patterns. For instance, in the weeks after SSWs there is usually increased precipitation over
46 Southern Europe while Northern Europe experiences more cold and dry weather conditions (Beerli
47 and Grams, 2019; King *et al.*, 2019). In addition to its importance for subseasonal and seasonal surface
48 variability, the SPV is also a driver of surface conditions on decadal time-scales (Kidston *et al.*, 2015).
49 In what way the SPV will change under global warming was further demonstrated to largely determine
50 future changes in European precipitation and extreme windiness (Karpechko and Manzini, 2012; Scaife
51 *et al.*, 2012; Zappa and Shepherd, 2017).

52 While the observed average effects of SSWs for Europe are well documented (Ayarzagüena *et al.*, 2018;
53 Kretschmer *et al.*, 2018a; King *et al.*, 2019; Afargan-Gerstman and Domeisen, 2020; Kautz *et al.*, 2020),
54 the surface impacts vary strongly across events. Only roughly half of the observed SSWs have been
55 classified as downward-propagating events, meaning that the stratospheric anomalies were followed
56 by the canonical NAO- response in the troposphere (Karpechko *et al.*, 2017). For the other events, so-
57 called non-downward propagating SSWs, the stratospheric circulation anomalies were mostly confined
58 to the stratosphere. As the exact downward coupling mechanisms of SSWs are not understood (e.g.
59 Hitchcock and Simpson, 2014) it is also not clear which factors modulate this difference.

60 To better understand the variability in the surface response of SSWs, several previous studies classified
61 SSWs according to different event characteristics. For example, SSWs have been distinguished by their
62 horizontal spatial structure (vortex split vs vortex displacement events), although no strong differences
63 in the tropospheric circulation response were found when analysing a large set of events in a climate
64 model (Maycock and Hitchcock, 2015). Moreover, differences in the troposphere-stratosphere
65 coupling mechanism have been addressed (absorptive vs reflective events), with the absorbing-type
66 events in particular being associated with downward-propagating SSWs and the canonical NAO-

67 surface response (Kodera *et al.*, 2016; Kretschmer *et al.*, 2018a; Matthias and Kretschmer, 2020).
68 Recent studies also tackled the importance of the prevailing North Atlantic weather regime during the
69 occurrence of SSWs and addressed how this modulates the surface response (Beerli and Grams, 2019;
70 Domeisen *et al.*, 2020). For example, Domeisen *et al.* (2020) found that high pressure anomalies over
71 Greenland (which project onto NAO-) are more likely to happen when the regime during the SSW onset
72 is a European Blocking regime (negative pressure anomalies over western Europe). Overall, several
73 factors likely contribute to the surface response, but which and how exactly remains an open question.

74 The purpose of this study is to investigate whether the *timing* of a SSW within the cold season (from
75 December to March) plays a role in the surface response. Such differences have been documented for
76 other drivers of European weather and climate, such as the El Niño Southern Oscillation (Jiménez-
77 Esteve and Domeisen, 2018; King *et al.*, 2021), but have as of yet not been documented for SSWs.
78 While SSWs are linked to a range of extreme events in different regions (Domeisen and Butler, 2020),
79 here we focus on anomalous temperature and precipitation in Europe.

80 Due to the limited observational record we make use of the large-ensemble hindcasts SEAS5 of the
81 seasonal prediction model from the European Centre for Medium-Range Weather Forecasts (ECMWF),
82 which provides a much larger sample of SSWs and allows us to address our research question with
83 statistical confidence (Stockdale *et al.*, 2018; Johnson *et al.*, 2019). In other words, instead of using the
84 model hindcasts to assess predictability, here we use hindcasts as a data archive to understand the
85 dynamical relationships (see also Byrne *et al.* (2019) for a similar approach). The assumption here is
86 that the mechanism behind stratosphere-troposphere coupling is reasonably well represented in
87 numerical weather prediction models and therefore the statistical surface response following SSWs
88 should be similar in models and observations.

89

90 **2 Data and methods**

91 **2.1 Data**

92 We use the ERA5 reanalysis dataset provided by ECMWF as observations (Hersbach *et al.*, 2020). We
93 use daily mean data from November 1981 to May 2019. The zonal wind velocity at 10 hPa is used to
94 detect SSWs, and the zonal wind velocity at 850 hPa as well as total precipitation and 2-meter
95 temperature is used to describe their surface impacts. Moreover, geopotential height data at 1000 hPa
96 and 150 hPa is used to study the downward propagation of SSWs.

97 Given the incomplete sampling of SSWs in the observations, output of the same variables from
98 ECMWF's seasonal forecasting model SEAS5 is further used (Stockdale *et al.*, 2018). Details of the

99 model configurations are described in Johnson et al. (2019). We use the 12-hourly output within the
100 extended winter season (November to April) from the re-forecasts initialized on the 1st of November
101 of each year from 1981 to 2018, from which we form daily means. The dataset contains 51 ensemble
102 members, thus providing 51 times more data over the same time period as compared to the
103 observations. In our analyses, we focus on the SEAS5 output from December onward, such that the
104 initial conditions play a minor role.

105 For all data, climatological anomalies are constructed by first removing the multi-year mean of each
106 day. For SEAS5 data, the multi-year mean over all ensemble members is subtracted. Note that the
107 multi-year mean is calculated for days of the same forecast lead-time relative to the initialization date,
108 resulting thus in 1-day shifted calendar days in March in leap years. The ERA5 dataset is interpolated
109 from a native TL639 grid (average grid-spacing of 30 km in the horizontal) onto the 0.25° latitude and
110 0.25° longitude grid. The SEAS5 precipitation and near-surface temperature data is interpolated from
111 a native TCo319 grid (average grid-spacing of 30 km in the horizontal) onto a 1° latitude and 1°
112 longitude grid, and the wind and geopotential height data is interpolated onto a 2.5° latitude and 2.5°
113 longitude grid.

114

115 **2.2 Methods**

116 We use the commonly applied definition of Charlton and Polvani (2007) to define SSWs. Accordingly,
117 a SSW is detected when the zonal-mean zonal wind at 60°N at 10 hPa from November to March is
118 below 0 m/s, i.e. the zonal-mean zonal wind is easterly (Charlton and Polvani, 2007). The first day this
119 value becomes negative is called the central date of the SSW. This definition further requires that no
120 other SSW is detected for at least 20 days after the winds have become positive again. This way, even
121 if the winds become westerly for a few days, the same event is not counted twice. Finally, the definition
122 requires that the zonal-mean zonal wind must return to positive for at least 10 consecutive days before
123 April 30th to ensure that SSWs are not mistaken for the final warming of the polar vortex.

124 To explore a potential role of differences in the downward coupling of SSWs to the troposphere, the
125 Northern Annular Mode (NAM) index is used. The NAM is calculated following Karpechko et al. (2017)
126 as the area-weighted average of daily mean geopotential height over the polar cap (60-90°N) for a
127 given pressure level. The index is then standardized by subtracting the multi-year climatology of each
128 day and dividing it by the daily multi-year standard deviation.

129 This standardized NAM index is used to classify SSWs into downward (dSSW) and non-downward
130 (nSSW) propagating events (Karpechko *et al.*, 2017; White *et al.*, 2019). Following Karpechko et al.

131 (2017), downward propagating events are those SSWs that fulfil the three following criteria: (1) the
132 1000 hPa NAM index (NAM1000) averaged over the 8 to 53 days after the SSW central date must be
133 negative, (2) at least 50% of all days within this 8 to 53 period must have a negative NAM1000 value,
134 (3) at least 70% of days within the 8 to 53 period must have a negative NAM150 value. Note that for
135 the third criteria we used the 150 hPa instead of the 100 hPa pressure level that was used in Karpechko
136 et al. (2017), as the latter is not part of the SEAS5 output. According to White et al. (2019) the use of
137 150 hPa leads to similar results.

138 To address the role of sampling uncertainty, we use a bootstrap approach following Byrne et al. (2019).
139 We generate 10,000 timeseries of length 38 years by randomly selecting one of the 51 ensemble
140 members for each year. From these 10,000 timeseries we then create a distribution of the studied
141 characteristics (e.g. the number of SSWs per winter month) and compare it to the observations (Byrne
142 *et al.*, 2019).

143

144 **3 Results**

145 **3.1 Model evaluation**

146 To first evaluate how well SEAS5 is capable of simulating the SPV and its variability, we compare its key
147 characteristics in the reanalysis with that of SEAS5. The SPV strength is here defined as the zonal-mean
148 zonal wind velocity at 60°N at 10 hPa. Fig. 1a shows the climatology (black thin line) as well as one and
149 two standard deviations (grey shadings) of the SPV over the course of the extended winter season.
150 Strong westerly winds are observed during the winter that peak in January when vortex variability is
151 also the largest. The winds then progressively slow down until turning on average negative in April.
152 Similar characteristics can be seen in the SEAS5 model, overall giving a smoothed picture due to the
153 larger number of data (Fig. 1b). In contrast to ERA5, the climatological wind is strongest in December
154 in the model.

155 We next calculate the number of SSWs per winter in both ERA5 and SEAS5 (Fig. 1c). In total 27 SSWs
156 occurred during the 38 considered winters from November 1981 to April 2019 in the observational
157 record, giving an average occurrence of 0.71 SSWs per winter. These events contain the same dates as
158 the list of 23 major SSWs provided in Karpechko et al. (2017) based on Era-Interim data, with two
159 additional events found on 17 February 2002 and 29 March 2008 in the ERA5 data set used here, as
160 well as on 20 March 2018 and 1 January 2019, which occurred after the above study was published. In
161 contrast, the 51 SEAS5 ensemble members contained 1705 events, giving an average of 0.88 SSWs per
162 winter.

163 To understand the role of sampling variability in Figs. 1 a-c we follow a bootstrap approach to create a
164 distribution of 10,000 time-series of length 38 years from the model ensemble and compare it to the
165 observations (see also Methods). We compute the mean (Fig. 1d) and the standard deviation (Fig. 1e)
166 of the SPV index over the course of the winter. The mean over all values is shown by the thin black
167 line, while that of the observations is indicated in red. The grey shadings indicate the 1%, 5%, 25%,
168 75%, 95% and 99% percentile thresholds. While observed SPV variability (red line in Fig. 1e) is well
169 within sampling uncertainty, the SPV mean in January lays outside the model spread (red line in Fig.
170 1d), suggesting that the mean strength is underestimated by the model during this time. Moreover,
171 we also compute the frequency of SSWs for all timeseries and show them in a box and whiskers plot
172 with the observations again indicated in red (Fig. 1f). Although the SSW frequency was found to be
173 lower in the observations (Fig. 1c), it is still consistent with sampling uncertainty. We further note that
174 the weak bias in the model in January (Fig. 1d) might contribute to the higher number of SSWs per
175 winter in SEAS5, since their detection depends on the absolute threshold of 0 m/s. Overall, Fig. 1 shows
176 that despite these differences, the SPV seasonal evolution and variability, including SSW frequency,
177 are well captured by SEAS5.

178 Next, we compare the surface impacts following SSWs in the model and the observations (Fig. 2). We
179 do this by plotting the zonal wind velocity anomalies at 850 hPa (u_{850} , Fig. 2a and 2b), the precipitation
180 anomalies (Fig. 2c and 2d) and the near-surface temperature anomalies (Fig. 2e and 2f) averaged over
181 the 30 days after the central date of all detected SSWs in the observations (Figs. 2a, c, e) and in SEAS5
182 (Figs. 2b, d, f). The observations show the expected negative NAO-type response. There are negative
183 wind anomalies over the North Atlantic and Scandinavia while wind anomalies over Southern Europe
184 are positive (Fig. 2a). This indicates southward shifted Atlantic storm tracks, transporting moist air to
185 Southern Europe. Consistently, precipitation anomalies over Southern and Central Europe are
186 anomalously high (Fig. 2c). In particular, the Iberian Peninsula as well as Italy and the Balkan region
187 show increased precipitation. In contrast, precipitation over Iceland, Ireland, Scotland and Norway is
188 on average anomalously low in the months after a SSW. Temperature anomalies are negative,
189 particularly over Scandinavia and similar patterns are found in SEAS5 (Fig. 2b, d, f). While negative wind
190 anomalies over the North Atlantic following SSWs are more pronounced in the model (Fig. 2b),
191 associated precipitation anomalies are less extreme in SEAS5 (Fig. 2d). Moreover, colder than average
192 temperatures are mostly confined to Northern Europe in SEAS5 (cf. Fig. 2e to Fig. 2f). Differences in
193 the response might at least partly be related to the higher numbers of events in the model compared
194 to the observations, which will tend to blur the effects of individual events. Moreover, it is possible
195 that some of the differences between SEAS5 and ERA5 are due to a better resolved orography in ERA5
196 (as it has higher spectral resolution than SEAS5).

197 In summary, Fig. 1 and Fig. 2 show that SEAS5 depicts polar vortex variability and the surface weather
198 impacts following SSWs reasonably well. This justifies our approach to use the SEAS5 model data to
199 study the role of SSW timing on precipitation impacts over Europe.

200

201 **3.2 The role of SSW timing on the surface response**

202 To investigate the role of the SSW timing on European precipitation, we first study the monthly
203 distribution of the frequency of SSWs. Fig. 3a shows the percentage of SSWs that occurred in a given
204 winter month, both for ERA5 (in red) and SEAS5 (in blue). We observe that SSWs are more likely to
205 occur in January and February (for ERA5 27% and 38% of all events) and less likely to occur in December
206 and March (for ERA5 13% and 20% of all events) both in the observations (ERA5) and in SEAS5. Unlike
207 the observations, SEAS5 contains a few events in November which we ignore in the following (see also
208 data section).

209 As before, the role of sampling uncertainty on the monthly occurrence rates is studied using a
210 bootstrap approach. Fig 3b shows the number of SSWs per month per winter in the 10,000 timeseries
211 using box and whiskers plots, with the observations indicated in red. On average, there are as many
212 SSWs in January as in February, and as many in December as in March, with the latter group having
213 much lower numbers of events than the former, consistent with Fig. 3a. Furthermore, we note that
214 the observations lie in the second quartile in December, February and March, and slightly below in
215 January. Thus, the differences between the model and the observations are again consistent with
216 sampling variability.

217 Similar to Fig. 2b, d, f we plot the u850, precipitation and temperature anomalies in SEAS5, averaged
218 over the 30 days after the SSW central date, this time separately for each month of SSW occurrence
219 (Fig. 4). The canonical negative NAO-type response is found for each month. That is, there are on
220 average windier and wetter weather conditions in Southern Europe, while Northern Europe
221 experiences less wind and rain but overall colder temperatures. Interestingly, the strength of the
222 anomalies weakens as the winter season progresses. While early winter (December and January, DJ)
223 events are followed by strong u850, precipitation and temperature anomalies, the response is less
224 pronounced in late winter (February and March, FM). For example, while average precipitation
225 anomalies over the Balkans in the month after a SSW occurring in December exceed 1 mm/d, they are
226 close to climatology after March SSWs. Similarly, rainfall is strongly decreased over Scotland after early
227 winter SSWs, while the signal is only weak after late winter events. For temperatures, the difference is
228 especially pronounced over Norway, where December SSWs are associated with temperature
229 anomalies of -1.3°C , whereas they only reach -0.2°C during SSWs occurring in March.

230 To investigate the difference between early and late winter SSWs in more detail, we compute regional
231 indices of precipitation anomalies for four regions particularly affected by SSWs (see Fig. 5a). We follow
232 King et al. (2019) and consider precipitation and temperature anomalies in Iberia and Eastern Europe
233 (which are both associated with anomalously high precipitation and temperatures after SSWs in
234 SEAS5), as well as over Scotland and Norway (which are both associated with anomalously low
235 precipitation and temperatures after SSWs). Note that the latter two regions are here smaller than the
236 regions considered by King et al. (2019). Figure 5b shows the 30 day-average following SSWs for each
237 region and month, normalised by the multi-year average of the month of the central date of the SSWs.
238 That is, precipitation anomalies following SSWs occurring in December are divided by the December
239 precipitation climatology, etc. Consistent with Fig. 4, the regional anomalies following SSWs - now
240 expressed as percentages of the monthly climatology - decrease over the course of the winter. For
241 example, after SSWs occurring in December there is on average 17% more precipitation in Iberia and
242 15% in Eastern Europe, compared to their December climatology. In contrast, SSWs occurring in March
243 only show an increase in 8.7% and 2.4% respectively of the climatology of that month. Similarly, the
244 anomalously low precipitation in Scotland and Norway decreases from 5.5% and 12% after December
245 SSWs to just 1.5% and 3.6% respectively after SSWs occurring in March. This means that the results in
246 Fig. 4 are not due to overall lower precipitation climatologies in late winter. These findings are also
247 robust (not shown) when normalising the precipitation anomalies by the 15 days shifted monthly
248 average (i.e., calculated from the 15th of the month of the central date up to the 15th of the following
249 month), to account for the fact that precipitation composites following SSWs also include days outside
250 of the month of the central date. We further plot the regional temperature anomalies (Fig. 5c) and find
251 a similar pattern. In all considered regions, early winter SSWs are associated with more pronounced
252 temperature anomalies than late winter SSWs. This difference is particularly striking over Norway.

253 We test how these findings compare to the observations, including whether the results are consistent
254 within sampling variability using a bootstrap approach. Figure 6 shows the observed precipitation
255 (expressed as percentages) and temperature anomalies in the four different regions after early (DJ,
256 dark blue bars) and late winter (FM, yellow bars) SSWs. We reduce our analysis to early and late winter
257 events here, to increase the analysed sample size of the observations. Except for Iberia, precipitation
258 anomalies in ERA5 are more pronounced after early winter SSWs (see Fig. 6a), consistent with Fig. 4
259 and 5. For observed temperatures, qualitatively similar differences between early and later winter
260 SSWs are found for Norway and Iberia but not for Scotland and Eastern Europe. Given the noise in the
261 observations, some inconsistency is to be expected. We further address this by showing the median
262 precipitation and temperature anomaly for the 10,000 time-series in SEAS5 (light blue and orange bars
263 in Fig. 6), with the black lines indicating the 5th and 95th confidence interval. While observed results

264 for precipitation in Scotland, Norway and Eastern Europe, as well as early winter results for Iberia are
265 well within sampling variability, the late winter SSW response for Iberia is not. Note, however, that the
266 confidence interval is widest for this region, indicating that sampling variability can at least somewhat
267 contribute to this difference. For Scotland and Norway, observed differences between early and late
268 winter SSWs are even more pronounced than in the model. For anomalous temperatures, the observed
269 early and later winter anomalies are also within sampling uncertainty, except for Eastern Europe
270 where the observed values lie just outside the range. Overall, despite the outlier of Iberian
271 precipitation after late winter SSWs, and temperatures in Eastern Europe, the observed precipitation
272 and temperature response following early and late winter SSWs is mostly consistent with SEAS5. Recall
273 that the confidence intervals are on the subsamples representative of the observations, just as in Figs.
274 1d-f and Fig 3b, indicating that the observations are consistent with the behaviour we see in the model.

275

276 **3.3 Regional risk of extreme events**

277 We further address how the timing of SSWs is related to the occurrence of extreme events. For
278 consistency with the previous results, we again analyse the 30 days averaged precipitation and
279 temperature anomalies after SSWs. Fig. 7 shows the probability density function of such anomalies for
280 early winter (blue) and late winter (orange) SSWs. The respective means are indicated by the dashed
281 lines and extreme percentiles of precipitation (10% for the British Isles and Southern Scandinavia, 90%
282 for Iberia and Eastern Europe) are shown by the dotted lines. Clearly, not only are the means of early
283 winter values separated in all regions, coherent with our previous findings (Fig. 4, 5), but also the
284 extreme values are more pronounced in each region after early winter SSWs. These results are also
285 consistent with those of King et al. (2019) for the observations.

286 To better quantify the risk of extreme events following early and late winter SSWs, we further compute
287 the risk ratios for each region. In order to do so, we computed the top and bottom 10% extreme 30-
288 day averaged precipitation and temperature anomalies for each region. The risk ratio is the probability
289 of an extreme event occurring after the central date of an early winter SSWs, divided by the probability
290 of it occurring after late winter SSWs. Here we find risk ratios of extremely low precipitation (below
291 the 10th percentile) of 1.7 Scotland and of 2.6 for Norway. This means, for example, that the risk of
292 extremely dry conditions is more than doubled in Norway after the occurrence of an early winter SSW
293 compared to that of a late winter SSW. Consistently, we find risk ratios of extremely high precipitation
294 (above the 90th percentile) of 1.7 both for Iberia and for Eastern Europe. For temperatures, risk ratios
295 for extremely low temperatures in Scotland and Norway are 1.1 and 1.4, while that of extreme high
296 temperatures in Iberia and Eastern Europe are 1 and 1.5. Thus, consistent with the previous analysis,

297 the risk of extreme anomalous precipitation is roughly increased by a factor of two after early winter
298 SSWs compared to that of late winter SSWs. For extreme temperatures, the risk is also increased
299 (except for Eastern Europe) but is less pronounced. Note that the risk of extreme events occurring in
300 the month after the central date of SSWs (regardless of month of occurrence) compared to months
301 with no SSWs are of comparable magnitude or even smaller. (For extreme precipitation, the risk ratios
302 are 0.8 and 1.1 for Scotland and Norway, and 1.5 and 1.3 for Iberia and Eastern Europe. For extreme
303 temperature, the risk ratios are 1.2 and 1.4 for Scotland and Norway, and 1 and 1.2 for Iberia and
304 Eastern Europe.).

305

306 **3.4 Are there more downward propagating SSWs in early winter?**

307 We now investigate a potential dynamical explanation for this difference between the early and late
308 winter SSW response. More precisely, we test if there are more SSWs that are downward propagating
309 to the troposphere in early winter than in late winter. This could explain the more pronounced surface
310 response in early winter, as downward propagating SSWs show by definition a stronger response in
311 the tropospheric circulation (Karpechko *et al.*, 2017). To test this hypothesis, we categorize each SSW
312 into either downward propagating (dSSWs) or non-downward propagating SSWs (nSSWs) (see also
313 Methods). We then first evaluate how well these properties are captured by the model. To do this we
314 plot the monthly share of dSSWs for both ERA5 and SEAS5 (see dashed line in Fig. 8a) and again address
315 the role of sampling uncertainty of this ratio using a bootstrap approach as before (Fig. 8b). We make
316 two observations.

317 Firstly, we find that there are more dSSWs in the observations than in SEAS5. In Fig. 8a only half of
318 January and February SSWs are downward propagating in the model, while more than 80% of those in
319 the observations are dSSWs. In contrast, the share of dSSWs in December in the model is twice as large
320 as that in the observations. Furthermore, there are some detected dSSWs in March in SEAS5 while
321 there are none in ERA5. The box and whiskers plots in Fig. 8b show that these rather strong differences
322 are yet still consistent with sampling uncertainty, albeit being on the outer edges of the distributions.

323 Secondly, Fig. 8a shows that there is no clear difference in the number of dSSWs occurring in early and
324 late winter. In fact, the percentage of dSSWs in SEAS5 in early winter (24% of all events) is
325 approximately the same as in late winter (20%). Thus, the ratio of dSSWs cannot explain the difference
326 between the early (DJ) and late winter (FM) SSW responses shown in Fig. 4. To confirm this, we also
327 plot the precipitation and temperature anomalies in the 30 days following only the dSSWs for each
328 month of the winter period (Fig. 8c). By construction, the precipitation and temperature anomalies are
329 now much more pronounced, as only the stratospheric events that reach the troposphere are included.

330 However, we still find that the anomalies are weaker after late winter SSWs. This confirms a role of the
331 timing of SSWs for their precipitation response that cannot be explained by different numbers of
332 downward-propagating SSW events.

333

334 **3.5. The role of the stratospheric mean state and event definition**

335 Finally, we assess the role of the stratospheric state in explaining the surface differences. We plot for
336 each winter month the SPV strength anomaly (measured as the zonal-mean zonal wind anomaly at
337 60°N at 10 hPa) during the central date of SSWs, against the associated surface response, here
338 measured in terms of the (non-standardized) NAM1000 index averaged 30 days after the central date
339 of the SSW. The scatter plot of the two quantities (see Fig. 9a) indicates an almost perfect linear
340 dependence ($r = 0.99$, $p < 0.01$, according to a two-sided Student t-test). We repeat the analyses using
341 the regional temperature and precipitation anomalies instead of the NAM1000 (not shown) and report
342 consistently high and statistically significant correlations (ranging from $r = -0.69$ for Iberian
343 temperatures to $r = 0.98$ for precipitation in Norway). Thus, the different monthly averaged NAM1000
344 responses (and consistently the precipitation and temperature anomalies) can entirely be explained
345 by differences in the strength of the stratospheric wind anomalies, with early winter SSWs being on
346 average associated with much stronger wind anomalies (-32 m/s in December, -26 m/s in January) than
347 later winter SSWs (-22 m/s in February, -16 m/s in March). In other words, the stronger the
348 stratospheric forcing, the stronger the surface response. While some previous studies concluded that
349 the surface response to SSWs does not correlate with the strength of mid- and upper stratospheric
350 anomalies (Runde *et al.*, 2016; Karpechko *et al.*, 2017), a similar dependence on the strength of the
351 stratospheric anomalies was also found in Polichtchouk *et al.* (2018) who varied the parametrized non-
352 orographic gravity wave drag strength in the ECMWF model. Furthermore, a dependence between
353 tropospheric circulation anomaly and precipitation anomaly has been reported (Zappa *et al.*, 2015;
354 Bevacqua *et al.*, 2021), consistent with our results.

355 We argue that while the relationship between SPV and NAM1000 anomalies is physical, the stronger
356 SPV anomalies during early winter SSWs (Fig. 9a) are a statistical artefact, directly related to the SSW
357 event criterion. Recall that a day is classified as a SSW when the stratospheric zonal-mean zonal wind
358 surpasses the *absolute* threshold of 0 m/s. However, the stratospheric mean state is stronger in early
359 than in late winter (see also black line in Fig. 1b). Thus, by selecting only those days where winds are
360 below 0 m/s, early winter events will have stronger wind *anomalies* (relative to the climatological mean
361 state). To test and visualize this effect, we first plot the daily SPV anomaly against the (30-day
362 averaged) NAM1000 anomalies for all winter days and find, as expected, a statistically significant

363 correlation (Fig. 9b, $r = 0.24$, $p < 0.01$). Importantly, there is, also as expected, no dependence on the
364 winter months (indicated by the different colours in the scatter plot), with anomalies spread similarly
365 across the different months (cf Fig. 1b). In contrast, when we repeat the plot for SSWs only, we find a
366 clear separation between the winter months, with the early winter SSWs (blue dots in Fig. 9c) showing
367 much stronger SPV anomalies, and therefore NAM1000 anomalies.

368 In statistics the effect discussed above is known as a selection or collider bias, and can be identified
369 with a causal network (Kretschmer *et al.*, 2021). The network in this case (Fig. 9d) illustrates the
370 assumed causal, i.e. physical, dependencies with the circles representing the involved variables and
371 the arrows indicating the presence and direction of an assumed causal influence. Here we assume a
372 causal chain from “SPV anomaly” to “NAM1000 anomaly” and further to “temperature/precipitation
373 anomaly”. Moreover, as argued before, both “SPV anomaly” and “month” affect the selection of
374 “SSW”, which in turn affects “NAM1000 anomaly”. The variable “SSW” is hence a common effect (also
375 called a collider) of “SPV anomaly” and “month” which are otherwise not statistically associated (see
376 Fig. 9b). By conditioning on, that is, selecting the common effect “SSW”, a spurious association
377 between “month” and “SPV anomaly” is introduced (see Fig. 9c).

378 In summary, while there is considerable spread across individual events (Fig. 9c), differences in the SPV
379 anomalies during SSWs in the winter months can fully explain the differences in the surface impacts
380 (Fig. 9a). The different SPV anomalies arise from the event definition of SSWs which does not account
381 for different mean states in the winter months.

382

383 **4 Discussion**

384 Our results suggest that the timing of SSWs plays an important role for their surface impacts, with early
385 winter SSWs being followed on average by stronger precipitation and temperature anomalies com-
386 pared to late winter SSWs. Here we tested if the number of downward propagating SSWs can explain
387 the different precipitation anomalies, but found this not to be the case. Similarly, the seasonal evolu-
388 tion of climatological precipitation cannot explain the differences.

389 Instead, a simple explanation for the surface differences of SSWs can be given by differences in the
390 SPV anomaly in different winter months, thus by the strength of the stratospheric forcing. Differences
391 in the forcing (and thereby the surface response) are a statistical artefact that is directly related to the
392 event definition of SSWs which involves an absolute threshold (of 0m/s), resulting in stronger SPV
393 anomalies during early winter events, where the stratospheric mean state is stronger.

394 Thus, caution is needed when interpreting surface impacts following SSWs (defined using an absolute
395 threshold) as, by construction, event averages will be dominated by the early winter events. Moreover,
396 deficits in climate models in capturing SSW frequencies may be related to the stratospheric mean state
397 being misrepresented (Polichtchouk *et al.*, 2018b). In a similar manner, changes in SSW frequency un-
398 der global warming can be the result of changes in the mean-state and not that of changes in the
399 vertical wave activity (McLandress and Shepherd, 2009). These examples stress why using *relative*
400 event criteria to study stratospheric extreme events can be beneficial (Hitchcock *et al.*, 2013; Kret-
401 schmer *et al.*, 2018a; Baldwin *et al.*, 2020). Nevertheless, there is of course a physical basis for an
402 absolute criterion, with the 0 m/s threshold implying that planetary waves (and stationary orographic
403 gravity waves) can no longer propagate into the stratosphere, thus changing stratospheric dynamics.
404 The appropriate event definition therefore depends on the guiding research question and it is im-
405 portant to bear both the physical and statistical characteristics of each in mind.

406 More generally, this study contributes to a larger body of literature arguing that seasonal-mean anal-
407 yses of teleconnections, and of stratosphere-troposphere coupling in particular, can blur over im-
408 portant details (Jiménez-Esteve and Domeisen, 2018; Kretschmer *et al.*, 2018a; King *et al.*, 2021). While
409 differences in the monthly surface response to SSWs were here demonstrated to be the result of the
410 SSW definition, other teleconnections and their seasonal dependencies might give further insights into
411 European climate variability. For example, the influence of La Niña on the NAO is mostly observed
412 during February but not during the other winter months (Jiménez-Esteve and Domeisen, 2018). Simi-
413 larly, the North Atlantic response to ENSO in late autumn was proposed to be different compared to
414 mid-winter (King *et al.*, 2021). Understanding how these other mechanisms are related to our findings
415 and contribute to differences in the surface response to SSWs is important but is beyond the scope of
416 the present study.

417 Finally, we note that although we found SEAS5 to reasonably well represent SSW frequency and down-
418 ward coupling characteristics, we cannot make direct inferences concerning the real world because of
419 sampling limitations in the observed record. For example, model biases (Tietsche *et al.*, 2020), as e.g.
420 in the SPV strength for January in SEAS5 might affect our results. Additional analysis showed that this
421 bias in January was not present in the SEAS5 data initialized on the 1st of December (not shown). The
422 observed increased precipitation in Iberia and high temperature anomalies in Eastern Europe after late
423 winter SSWs were more pronounced than in the model but the reasons for that were not investigated
424 here. Testing our findings in other models and for shorter lead-times, e.g. such as in models participat-
425 ing in the S2S project (Vitart and Robertson, 2018), is therefore an important next step.

426

427 **5 Summary and Conclusions**

428 Sudden Stratospheric Warmings (SSWs) strongly impact European winter weather. This study analysed
429 the role played by the timing of SSWs within the winter season on the precipitation and temperature
430 response over Europe. To address this question we capitalized on the large ensemble hindcasts of the
431 ECMWF seasonal forecast model SEAS5 initialized on the 1st of November of each year, providing a
432 bigger archive of SSWs.

433 We analysed how well the model captures key stratospheric characteristics such as mean stratospheric
434 wind velocity and variability (Fig. 1), average frequency of SSWs (Fig. 3) as well as the number of down-
435 ward propagating SSWs (Fig. 8a,b), and found the model to reasonably capture the expected proper-
436 ties, with differences from the observations being mostly within sampling uncertainty. Moreover, we
437 tested how well the precipitation, temperature and zonal wind velocities at 850 hPa after SSWs in the
438 model resembled those in the observations (Fig. 2). While there were some differences, in particular
439 regarding the North Atlantic wind anomalies, overall we found the model to well represent the surface
440 impacts related to SSWs.

441 The analysis of the timing in SEAS5 suggested a difference between early (DJ) and late (FM) winter
442 events. We found that early winter SSWs have a stronger impact on European weather, with higher
443 precipitation and temperature anomalies (Fig. 4, 5). In contrast, late winter events have a smaller in-
444 fluence on surface weather. For example, while precipitation after December SSWs in Norway is re-
445 duced by approximately 12% of the monthly climatology, a reduction of only 4% was found after SSWs
446 occurring in March. Except for Iberia, these results are consistent with the observed response of SSWs,
447 despite the limited sample size (Fig. 6). Consistently, the risk of extreme precipitation anomalies, and
448 similarly that of extreme temperature anomalies in the month after the occurrence of SSWs is in-
449 creased after early winter SSWs (Fig. 7).

450 We showed that this difference between early and late winter events cannot be explained by a differ-
451 ent number of downward propagating SSWs, which were here found to be similar for early and later
452 winter (Fig. 8). Instead, differences are the result of the commonly used SSW event definition which
453 involves an absolute threshold, thereby favouring stronger events (in terms of anomalous SPV
454 strength) in early winter when the stratospheric mean state is stronger (Fig. 9). Overall, this study thus
455 demonstrates the role of SSW event definition in affecting surface impacts.

456

457 **Acknowledgments**

458 We thank Ted Shepherd and Emanuele Bevacqua for useful feedback and discussions. We further
459 thank two anonymous reviewers for constructive feedback which helped to improve the manuscript.

460

461 **Funding information**

462 M.K. has received funding from the European Union's Horizon 2020 research and innovation
463 programme under the Marie Skłodowska-Curie grant agreement (No 841902).

464 **References**

- 465 Afargan-Gerstman H, Domeisen DIV. 2020. Pacific Modulation of the North Atlantic Storm Track
466 Response to Sudden Stratospheric Warming Events. *Geophysical Research Letters*. Blackwell
467 Publishing Ltd, 47(2). <https://doi.org/10.1029/2019GL085007>.
- 468 Ayarzagüena B, Barriopedro D, Garrido-Perez JM, Abalos M, de la Cámara A, García-Herrera R, Calvo
469 N, Ordóñez C. 2018. Stratospheric Connection to the Abrupt End of the 2016/2017 Iberian Drought.
470 *Geophysical Research Letters*. Blackwell Publishing Ltd, 45(22): 12,639-12,646.
471 <https://doi.org/10.1029/2018GL079802>.
- 472 Baldwin MP, Ayarzagüena B, Birner T, Butchart N, Charlton-Perez AJ, Butler AH, Domeisen DIV,
473 Garfinkel CI, Garny H, Gerber EP, Hegglin MI, Langematz U, Pedatella NM. 2020. *Sudden Stratospheric*
474 *Warmings*. *Earth and Space Science Open Archive*. preprint. Earth and Space Science Open Archive.
- 475 Baldwin MP, Dunkerton TJ. 2001. Stratospheric harbingers of anomalous weather regimes. *Science*
476 *(New York, N.Y.)*. American Association for the Advancement of Science, 294(5542): 581–4.
477 <https://doi.org/10.1126/science.1063315>.
- 478 Beerli R, Grams CM. 2019. Stratospheric modulation of the large-scale circulation in the Atlantic–
479 European region and its implications for surface weather events. *Quarterly Journal of the Royal*
480 *Meteorological Society*. John Wiley and Sons Ltd, 145(725): 3732–3750.
481 <https://doi.org/10.1002/qj.3653>.
- 482 Bevacqua E, Shepherd TG, Watson PAG, Sparrow S, Wallom D, Mitchell D. 2021. Larger Spatial
483 Footprint of Wintertime Total Precipitation Extremes in a Warmer Climate. *Geophysical Research*
484 *Letters*, 48(8). <https://doi.org/10.1029/2020GL091990>.
- 485 Byrne NJ, Shepherd TG, Polichtchouk I. 2019. Subseasonal-to-Seasonal Predictability of the Southern
486 Hemisphere Eddy-Driven Jet During Austral Spring and Early Summer. *Journal of Geophysical*
487 *Research: Atmospheres*. Blackwell Publishing Ltd, 124(13): 2018JD030173.
488 <https://doi.org/10.1029/2018JD030173>.
- 489 Charlton AJ, Polvani LM. 2007. A New Look at Stratospheric Sudden Warmings. Part I: Climatology
490 and Modeling Benchmarks. *Journal of Climate*, 20(3): 449–469. <https://doi.org/10.1175/JCLI3996.1>.
- 491 Domeisen DI V., Butler AH. 2020. Stratospheric drivers of extreme events at the Earth’s surface.
492 *Communications Earth & Environment*. Springer Science and Business Media LLC, 1(1): 1–8.
493 <https://doi.org/10.1038/s43247-020-00060-z>.
- 494 Domeisen DI V., Grams CM, Papritz L. 2020. The role of North Atlantic–European weather regimes in
495 the surface impact of sudden stratospheric warming events. *Weather and Climate Dynamics*.
496 Copernicus GmbH, 1(2): 373–388. <https://doi.org/10.5194/wcd-1-373-2020>.
- 497 Hersbach H, Bell B, Berrisford P, Hirahara S, Horányi A, Muñoz-Sabater J, Nicolas J, Peubey C, Radu R,
498 Schepers D, Simmons A, Soci C, Abdalla S, Abellan X, Balsamo G, Bechtold P, Biavati G, Bidlot J,
499 Bonavita M, Chiara G, Dahlgren P, Dee D, Diamantakis M, Dragani R, Flemming J, Forbes R, Fuentes
500 M, Geer A, Haimberger L, Healy S, Hogan RJ, Hólm E, Janisková M, Keeley S, Laloyaux P, Lopez P, Lupu
501 C, Radnoti G, Rosnay P, Rozum I, Vamborg F, Villaume S, Thépaut J. 2020. The ERA5 Global
502 Reanalysis. *Quarterly Journal of the Royal Meteorological Society*. Wiley, qj.3803.
503 <https://doi.org/10.1002/qj.3803>.

504 Hitchcock P, Shepherd TG, Manney GL. 2013. Statistical Characterization of Arctic Polar-Night Jet
505 Oscillation Events. *Journal of Climate*. American Meteorological Society, 26(6): 2096–2116.
506 <https://doi.org/10.1175/JCLI-D-12-00202.1>.

507 Hitchcock P, Simpson IR. 2014. The Downward Influence of Stratospheric Sudden Warmings. *Journal*
508 *of the Atmospheric Sciences*, 71(10): 3856–3876. <https://doi.org/10.1175/JAS-D-14-0012.1>.

509 Jiménez-Esteve B, Domeisen DI V. 2018. The Tropospheric Pathway of the ENSO–North Atlantic
510 Teleconnection. *Journal of Climate*, 31(11): 4563–4584. <https://doi.org/10.1175/JCLI-D-17-0716.1>.

511 Johnson SJ, Stockdale TN, Ferranti L, Balmaseda MA, Molteni F, Magnusson L, Tietsche S, Decremmer
512 D, Weisheimer A, Balsamo G, Keeley SPE, Mogensen K, Zuo H, Monge-Sanz BM. 2019. SEAS5: The
513 new ECMWF seasonal forecast system. *Geoscientific Model Development*. Copernicus GmbH, 12(3):
514 1087–1117. <https://doi.org/10.5194/gmd-12-1087-2019>.

515 Karpechko AY, Manzini E. 2012. Stratospheric influence on tropospheric climate change in the
516 Northern Hemisphere: STRATOSPHERIC IMPACT ON CLIMATE CHANGE. *Journal of Geophysical*
517 *Research: Atmospheres*, 117(D5): n/a-n/a. <https://doi.org/10.1029/2011JD017036>.

518 Karpechko AY, Hitchcock P, Peters DHW, Schneidereit A. 2017. Predictability of downward
519 propagation of major sudden stratospheric warmings. *Quarterly Journal of the Royal Meteorological*
520 *Society*. John Wiley & Sons, Ltd. <https://doi.org/10.1002/qj.3017>.

521 Kautz L, Polichtchouk I, Birner T, Garny H, Pinto JG. 2020. Enhanced extended-range predictability of
522 the 2018 late-winter Eurasian cold spell due to the stratosphere. *Quarterly Journal of the Royal*
523 *Meteorological Society*. John Wiley and Sons Ltd, 146(727): 1040–1055.
524 <https://doi.org/10.1002/qj.3724>.

525 Kidston J, Scaife AA, Hardiman SC, Mitchell DM, Butchart N, Baldwin MP, Gray LJ. 2015. Stratospheric
526 influence on tropospheric jet streams, storm tracks and surface weather. *Nature Geoscience*, 8(6):
527 433–440. <https://doi.org/10.1038/ngeo2424>.

528 King AD, Butler AH, Jucker M, Earl NO, Rudeva I. 2019. Observed Relationships Between Sudden
529 Stratospheric Warmings and European Climate Extremes. *Journal of Geophysical Research:*
530 *Atmospheres*. Blackwell Publishing Ltd, 124(24): 13943–13961.
531 <https://doi.org/10.1029/2019JD030480>.

532 King MP, Li C, Sobolowski S. 2021. Resampling of ENSO teleconnections: accounting for cold season
533 evolution reduces uncertainty in the North Atlantic. *Weather and Climate Dynamics Discussions*.
534 Copernicus GmbH, 1–24. <https://doi.org/10.5194/wcd-2021-15>.

535 Kodera K, Mukougawa H, Maury P, Ueda M, Claud C. 2016. Absorbing and reflecting sudden
536 stratospheric warming events and their relationship with tropospheric circulation. *Journal of*
537 *Geophysical Research: Atmospheres*, 121(1): 80–94. <https://doi.org/10.1002/2015JD023359>.

538 Kretschmer M, Adams SV, Arribas A, Prudden R, Robinson N, Saggioro E, Shepherd TG. 2021.
539 Quantifying causal pathways of teleconnections. *Bulletin of the American Meteorological Society*.
540 American Meteorological Society, 1(aop): 1–34. <https://doi.org/10.1175/BAMS-D-20-0117.1>.

541 Kretschmer M, Cohen J, Matthias V, Runge J, Coumou D. 2018a. The different stratospheric influence
542 on cold-extremes in Eurasia and North America. *npj Climate and Atmospheric Science*. Nature
543 Publishing Group, 1(1): 44. <https://doi.org/10.1038/s41612-018-0054-4>.

544 Kretschmer M, Coumou D, Agel L, Barlow M, Tziperman E, Cohen J. 2018b. More-Persistent Weak
545 Stratospheric Polar Vortex States Linked to Cold Extremes. *Bulletin of the American Meteorological*
546 *Society*, 99(1): 49–60. <https://doi.org/10.1175/BAMS-D-16-0259.1>.

547 Matthias V, Kretschmer M. 2020. The influence of stratospheric wave reflection on North American
548 cold spells. *Monthly Weather Review*. American Meteorological Society, 148(4): 1675–1690.
549 <https://doi.org/10.1175/MWR-D-19-0339.1>.

550 Maycock AC, Hitchcock P. 2015. Do split and displacement sudden stratospheric warmings have
551 different annular mode signatures? *Geophysical Research Letters*, 42(24): 10,943–10,951.
552 <https://doi.org/10.1002/2015GL066754>.

553 McLandress C, Shepherd TG. 2009. Impact of Climate Change on Stratospheric Sudden Warmings as
554 Simulated by the Canadian Middle Atmosphere Model. *Journal of Climate*. American Meteorological
555 Society, 22(20): 5449–5463. <https://doi.org/10.1175/2009JCLI3069.1>.

556 Polichtchouk I, Shepherd TG, Byrne NJ. 2018a. Impact of Parametrized Nonorographic Gravity Wave
557 Drag on Stratosphere-Troposphere Coupling in the Northern and Southern Hemispheres. *Geophysical*
558 *Research Letters*, 45(16): 8612–8618. <https://doi.org/10.1029/2018GL078981>.

559 Polichtchouk I, Shepherd TG, Hogan RJ, Bechtold P. 2018b. Sensitivity of the Brewer–Dobson
560 Circulation and Polar Vortex Variability to Parameterized Nonorographic Gravity Wave Drag in a
561 High-Resolution Atmospheric Model. *Journal of the Atmospheric Sciences*. American Meteorological
562 Society, 75(5): 1525–1543. <https://doi.org/10.1175/JAS-D-17-0304.1>.

563 Runde T, Dameris M, Garny H, Kinnison DE. 2016. Classification of stratospheric extreme events
564 according to their downward propagation to the troposphere: CLASSIFICATION OF STRATOSPHERIC
565 EVENTS. *Geophysical Research Letters*, 43(12): 6665–6672. <https://doi.org/10.1002/2016GL069569>.

566 Scaife AA, Spanghel T, Fereday DR, Cubasch U, Langematz U, Akiyoshi H, Bekki S, Braesicke P,
567 Butchart N, Chipperfield MP, Gettelman A, Hardiman SC, Michou M, Rozanov E, Shepherd TG. 2012.
568 Climate change projections and stratosphere–troposphere interaction. *Climate Dynamics*, 38(9–10):
569 2089–2097. <https://doi.org/10.1007/s00382-011-1080-7>.

570 Stockdale T, Johnson S, Ferranti L, Balamseda M, Briceag S. 2018. ECMWF’s new long-range
571 forecasting system SEAS5. *ECMWF Newsletter*, (154).

572 Tietsche S, Balmaseda M, Zuo H, Roberts C, Mayer M, Ferranti L. 2020. The importance of North
573 Atlantic Ocean transports for seasonal forecasts. *Climate Dynamics*, 55(7): 1995–2011.
574 <https://doi.org/10.1007/s00382-020-05364-6>.

575 Vitart F, Robertson AW. 2018. The sub-seasonal to seasonal prediction project (S2S) and the
576 prediction of extreme events. *npj Climate and Atmospheric Science*. Springer US, 1(1): 1–7.
577 <https://doi.org/10.1038/s41612-018-0013-0>.

578 Waugh DW, Sobel AH, Polvani LM. 2016. What is the Polar Vortex, and how does it influence
579 weather? *Bulletin of the American Meteorological Society*, BAMS-D-15-00212.1.
580 <https://doi.org/10.1175/BAMS-D-15-00212.1>.

581 White I, Garfinkel CI, Gerber EP, Jucker M, Aquila V, Oman LD. 2019. The downward influence of
582 sudden stratospheric warmings: Association with tropospheric precursors. *Journal of Climate*.
583 American Meteorological Society, 32(1): 85–108. <https://doi.org/10.1175/JCLI-D-18-0053.1>.

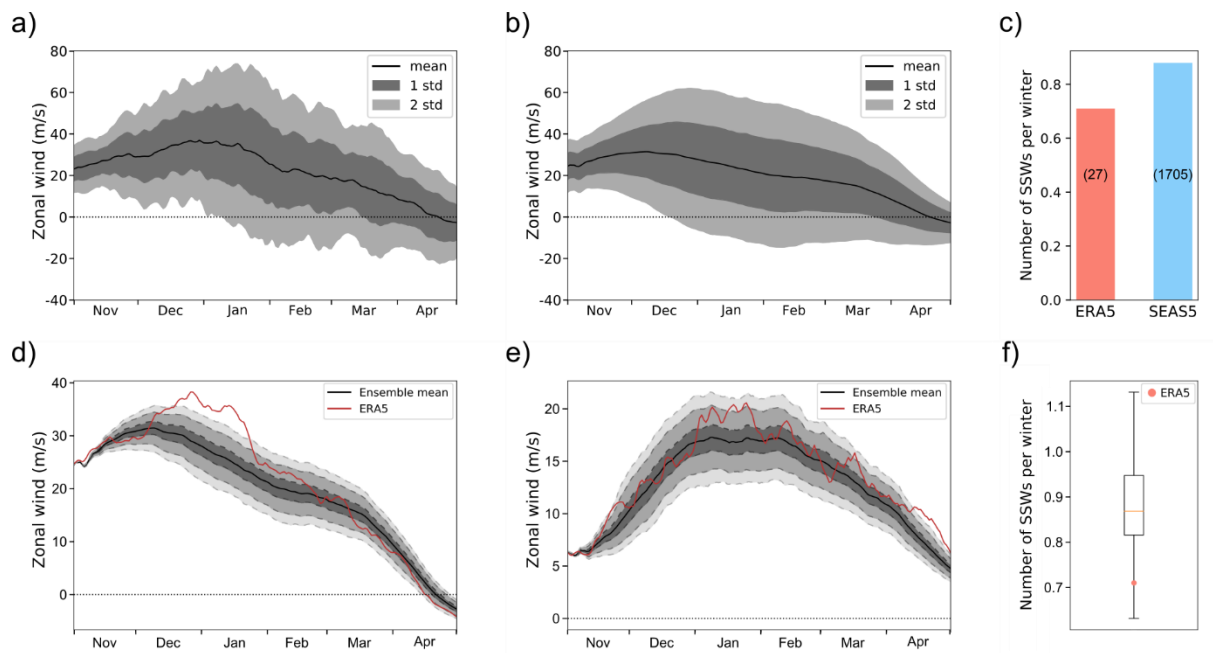
584 Zappa G, Hoskins BJ, Shepherd TG. 2015. The dependence of wintertime Mediterranean precipitation
585 on the atmospheric circulation response to climate change. *Environmental Research Letters*. IOP
586 Publishing, 10(10): 104012. <https://doi.org/10.1088/1748-9326/10/10/104012>.

587 Zappa G, Shepherd TG. 2017. Storylines of Atmospheric Circulation Change for European Regional
588 Climate Impact Assessment. *Journal of Climate*. American Meteorological Society, 30(16): 6561–
589 6577. <https://doi.org/10.1175/JCLI-D-16-0807.1>.

590

591 **Figures**

592



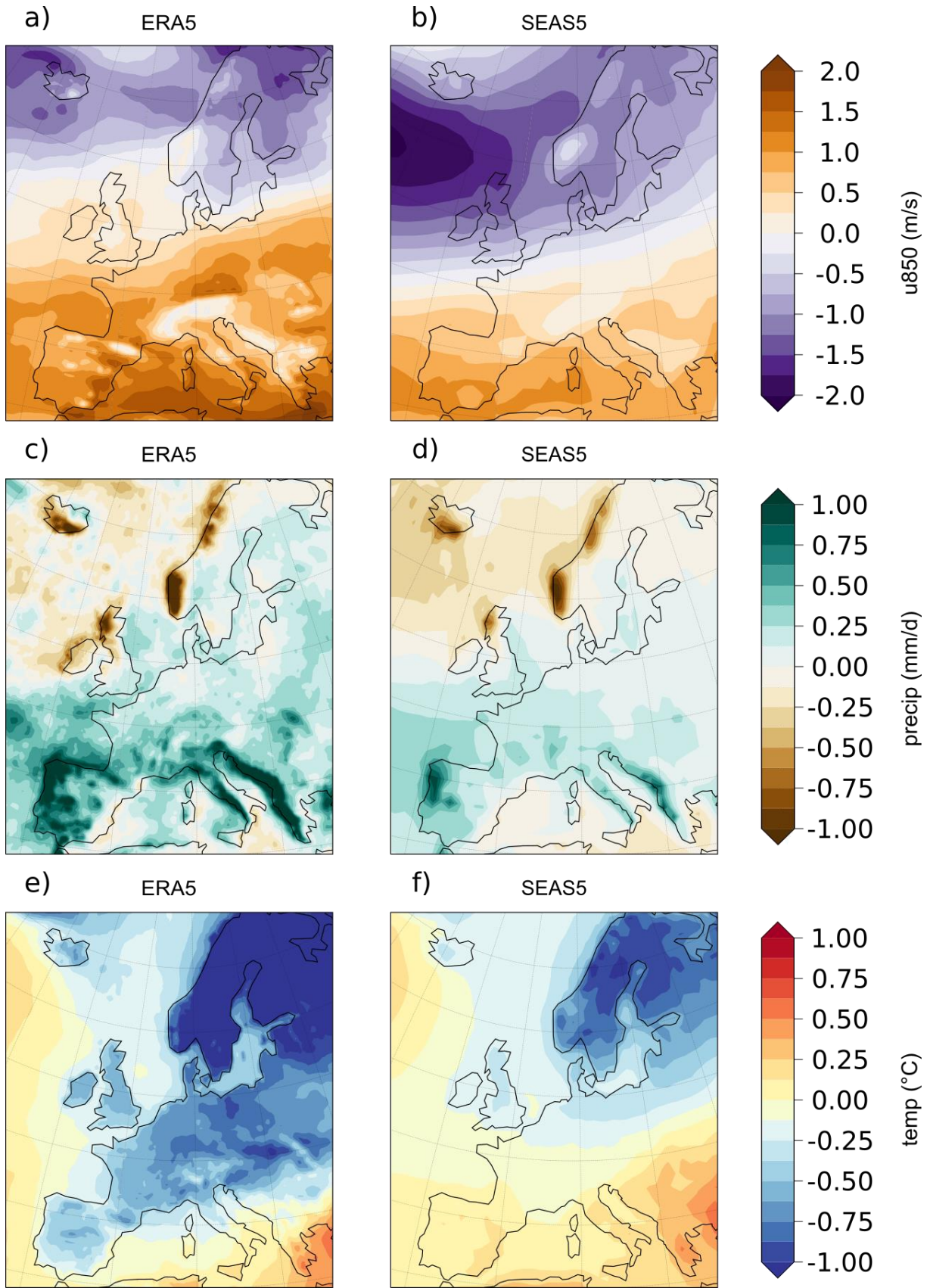
593

594

595 **FIGURE 1.** Comparison between the SPV in the observational record (ERA5) and the model dataset
 596 (SEAS5). (a) and (b) Climatology of the SPV, defined as the zonal-mean zonal wind velocity at 60°N at
 597 10 hPa (thin black line) for ERA5 and SEAS5, respectively. The dark and light grey shadings correspond
 598 to the one and two standard deviation. (c) Number of SSWs per winter for ERA5 (red) and SEAS5 (blue).
 599 The raw number of SSWs is indicated in brackets on the bars. (d) Bootstrap estimate of sampling un-
 600 certainty associated with 38-year mean of the SPV. The bootstrap estimate was generated using 10,000
 601 timeseries of length 38 and randomly choosing one ensemble member for each year. Dashed lines
 602 represent the 1st, 5th, 25th, 75th, 95th and 99th percentiles. The red line corresponds to ERA5 observa-
 603 tions. (e) Same as (d) but computing the SPV standard deviation instead of the mean. (f) Number of
 604 SSWs per winter in the 10,000 timeseries. The orange line indicates the median, the box indicates the
 605 quartiles, and the whiskers show the 5th and 95th percentiles. The red dot indicates the observational
 606 value.

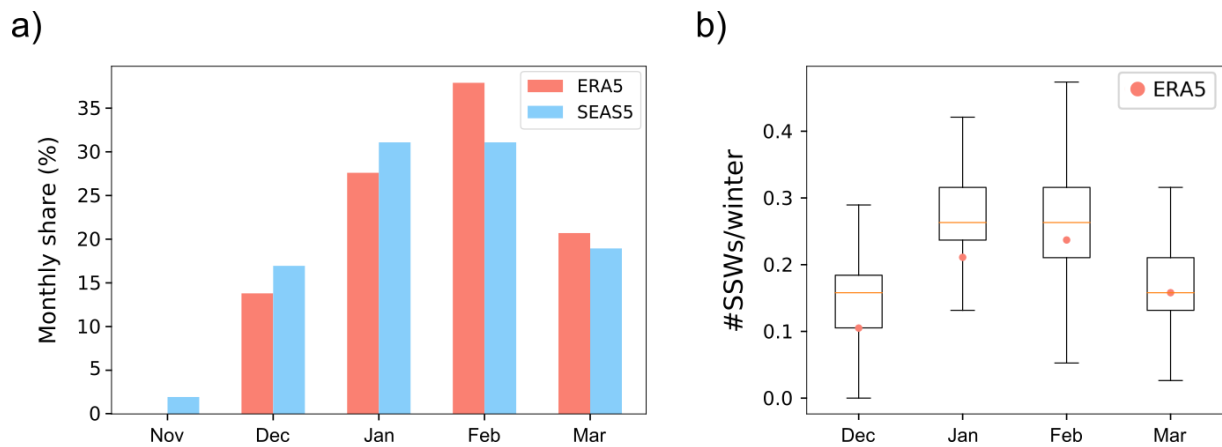
607

608



610 **FIGURE 2.** Tropospheric response to SSWS. The panels show the 30-days averages of u850 (top row),
611 precipitation (middle row) and temperature (bottom row) anomalies after the SSW central date, aver-
612 aged over all SSWs in ERA5 (panels a, c, e) and SEAS5 (panels b, d, f).

613

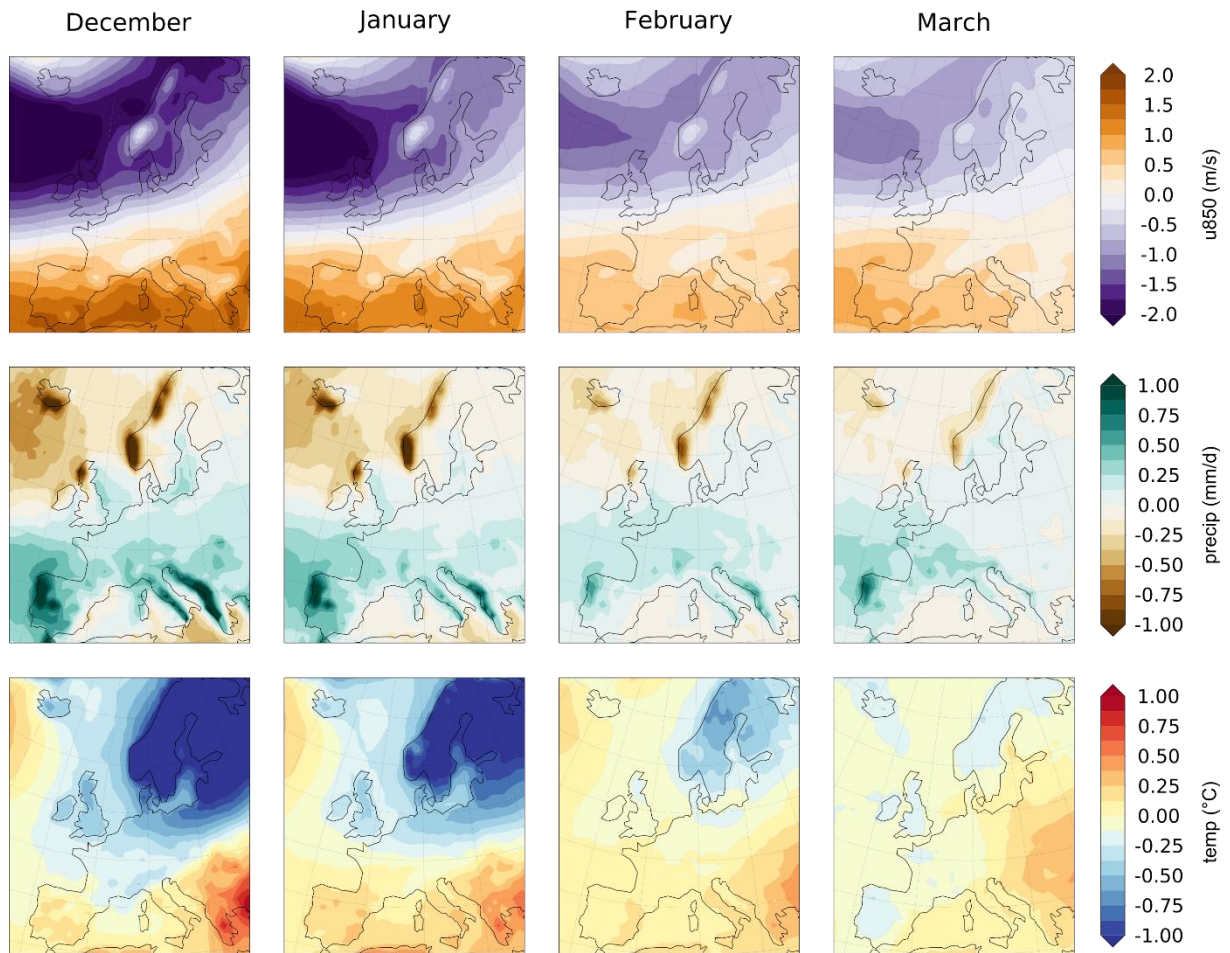


614

615

616 **FIGURE 3.** Representation of the SSW timing. (a) Number of SSWs per month, shown as a fraction of
617 all the events for ERA5 (red) and SEAS5 (blue) for each month of the winter season. (b) Distribution of
618 the number of SSWs per winter month, calculated for the 10,000 model timeseries. The orange lines
619 indicate the median, the boxes indicate the quartiles, and the whiskers show the 5th and 95th percen-
620 tiles. The red dots are the observed values.

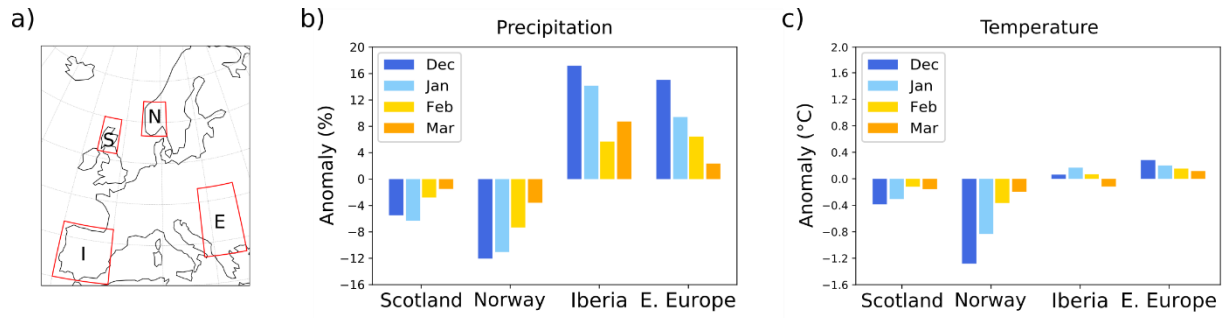
621



622

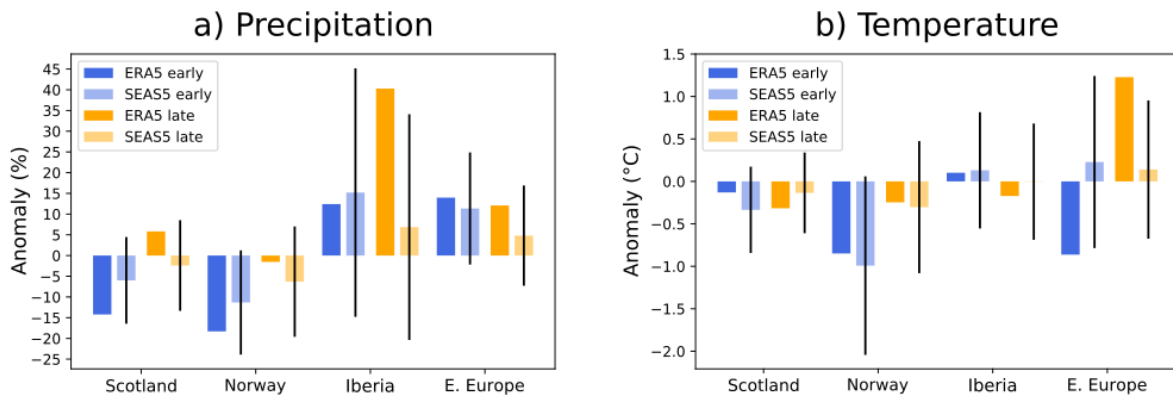
623 **FIGURE 4.** Tropospheric response to SSWs split by month. 30-days averages of u850 (top row), precip-
 624 itation (middle row), and temperature (bottom row) anomalies after the SSW central date for each
 625 month in the winter season for SEAS5.

626



627

628 **FIGURE 5.** Regional precipitation anomalies. (a) Map of Europe showing the four regions (red rectan-
 629 gles) over which regional indices are calculated: Scotland (6.5-1.5 °W, 55-60°N), Norway (4.5-11.5 °E,
 630 58-63°N), Iberia (10°W-1°E, 36-44°N), Eastern Europe (18-26 °E, 40-50°N). (b) 30-days averaged pre-
 631 cipitation anomalies following SSWs normalized by the multi-year monthly climatology, for each region
 632 and each month of the winter season. (c) 30-days averaged temperature anomalies following SSWs,
 633 for each region and each month of the winter season.

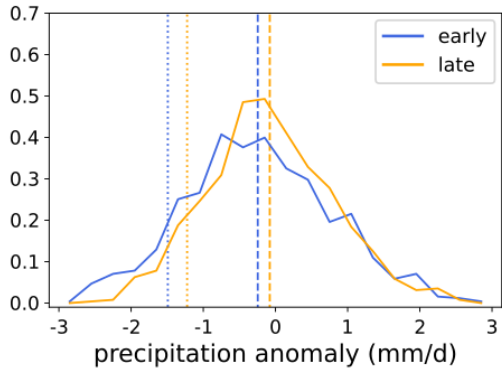


634

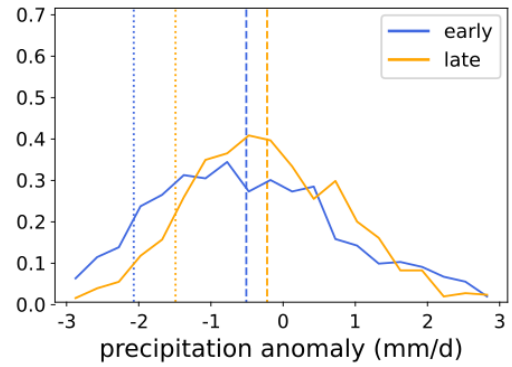
635 **FIGURE 6.** Consistency with the observations and the role of sampling uncertainty. 30-days averaged
 636 anomalies following SSWs for each region and split by early or late winter occurrence for a) precipita-
 637 tion (normalized by the multi-year early (DJ) and late winter (FM) climatology), and b) temperature.
 638 The observations are shown by the dark blue and yellow bars. The light blue and orange bars show the
 639 results for the model, with the height of the bars indicating the median of the 10,000 timeseries (see
 640 methods) and the black lines indicating the 5th and 95th percentile.

Precipitation

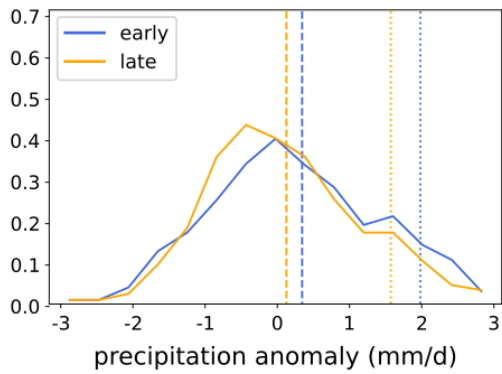
a) Scotland



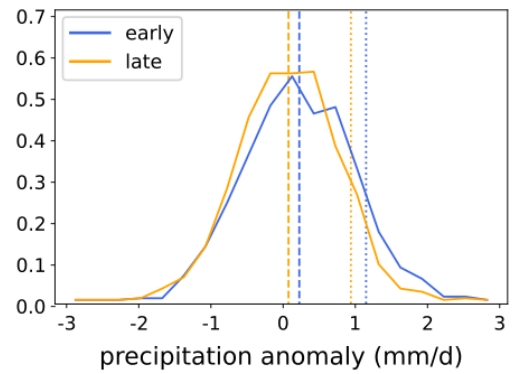
b) Norway



c) Iberia

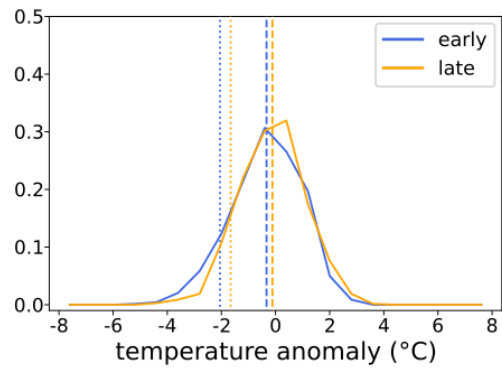


d) Eastern Europe

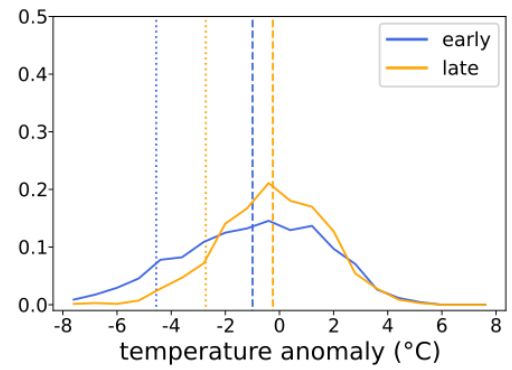


Temperature

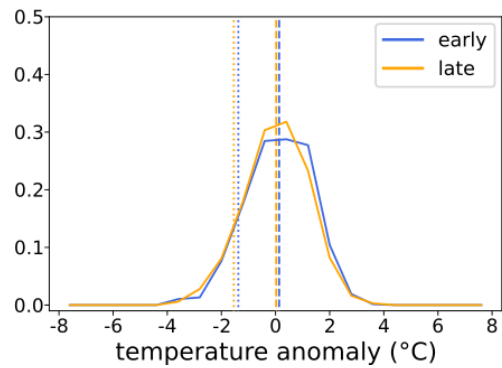
e) Scotland



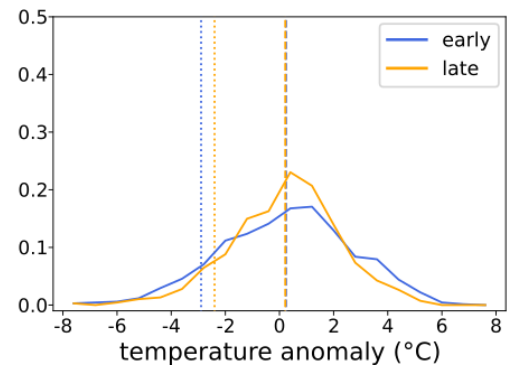
f) Norway



g) Iberia

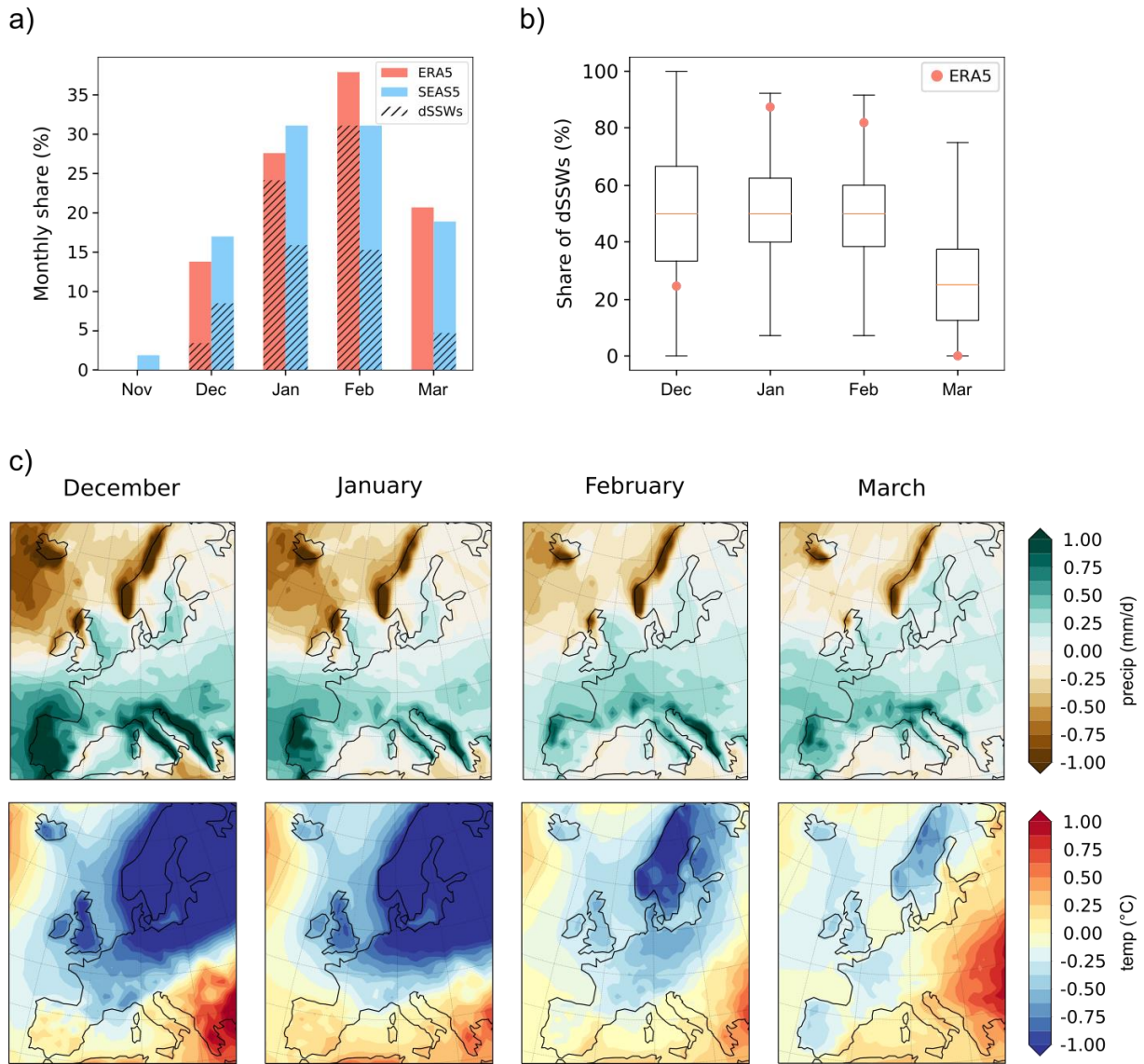


h) Eastern Europe



642 **FIGURE 7.** Probability density functions of 30-days averaged precipitation anomalies following early
643 winter SSWs (blue) and late winter SSWs (orange) for (a) Scotland, (b) Norway, (c) Iberia and (d) Eastern
644 Europe (see Figure 5 for details on the regions). The dashed lines show the average precipitation anom-
645 alies and the dotted lines show the 10th (a,b) and 90th (c,d) percentiles. e)-h) same as a)-d) but for
646 temperature anomalies instead of temperature.

647



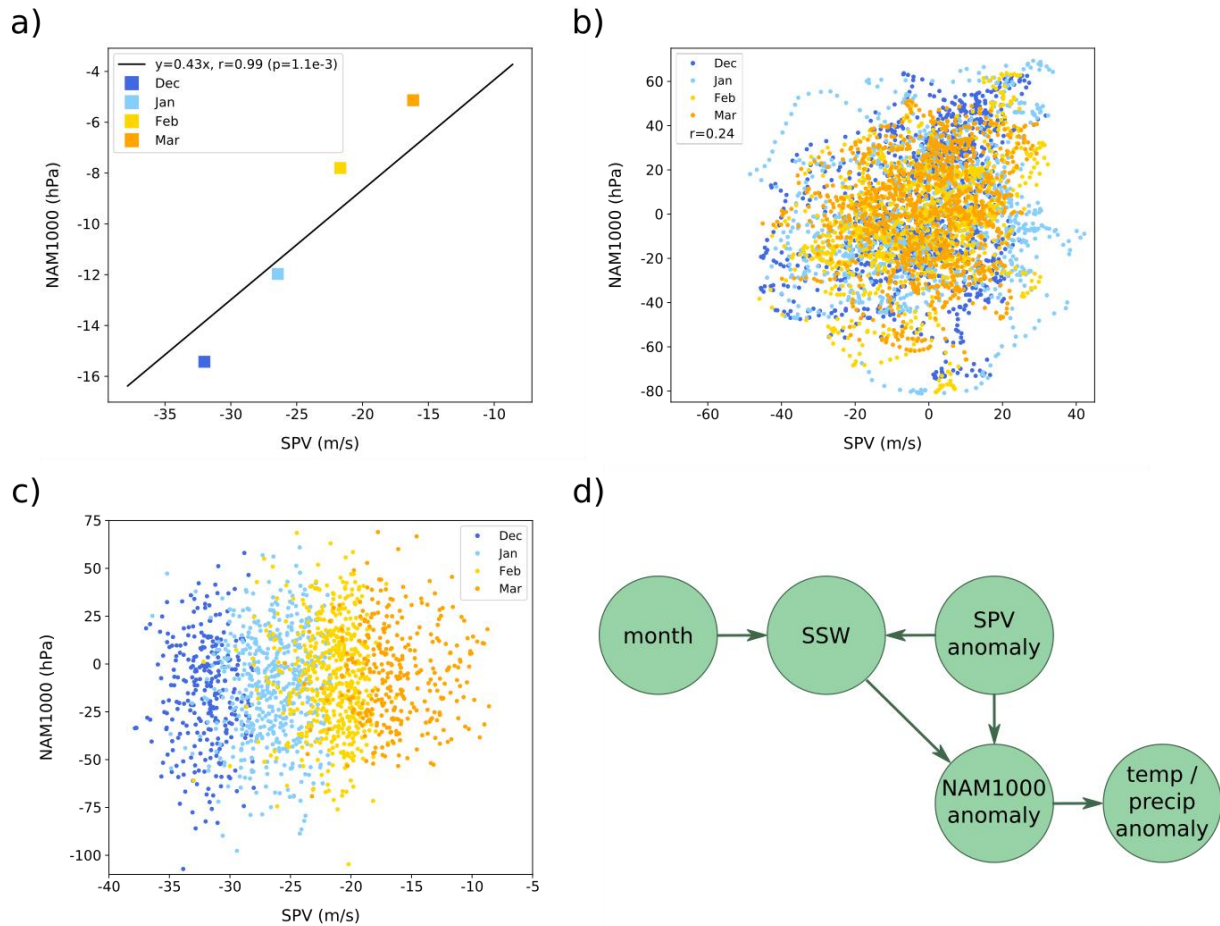
648

649

650 **FIGURE 8.** The role of downward propagation of SSWs (dSSWs). (a) Proportion of dSSWs per month
 651 (dashed) for ERA5 (red) and SEAS5 (blue) for each month in winter. (b) Share of dSSWs of all SSWs per
 652 month in the 10,000 model timeseries. Orange lines are the medians over all timeseries. Red dots are
 653 the observed values. The whiskers indicate the 5th and 95th percentiles. (c) Same as in Fig. 4 but for
 654 dSSWs in SEAS5 only.

655

656



657

658

659 **FIGURE 9.** The role of the stratospheric state. (a) Scatter plot of the SPV anomaly during the central
 660 date of SSWs for each month and the according (non-standardized) NAM1000 anomaly averaged 30-
 661 days after the central dates in SEAS5. The black line indicated the regression line resulting from fitting
 662 $y = \text{NAM1000}$ on $x = \text{SPV}$. (b) Scatter plot of SPV anomalies during all winter days and the according
 663 (non-standardized) NAM1000 anomalies averaged in the following 30-days. The different colours indi-
 664 cate the different winter months, see legend. To aid visualization, we only show SPV and NAM1000
 665 anomalies of the first ensemble member. (c) Same as (b) but for SSWs only and using all ensemble
 666 members. (d) Causal network representing the involved causal dependencies. The SPV anomaly is as-
 667 summed to affect the NAM1000 anomaly which affects the temperature and precipitation anomaly in
 668 Europe. SSWs are defined as when the zonal-mean zonal wind anomaly is negative, with the strength
 669 of the mean-state varying across the winter. Therefore, the occurrence of a SSW is influenced both by
 670 the SPV anomaly as well as the month. Just as SPV anomalies in general, SSWs also affect the NAM1000
 671 anomaly.